PNAS RESEARCH ARTICLE | IMMUNOLOGY AND INFLAMMATION OPEN ACCESS

Deficiency in platelet 12-lipoxygenase exacerbates inflammation and disease severity during SARS-CoV-2 infection

Ana Claudia dos S. P. Andrade[a], Emile Lacasse[a], Isabelle Dubuc[a], Leslie Gudimard[a], Annie Gravel[a], Florian Puhm[a], Gabriel Campolina-Silva[b], Celso Queiroz-Junior[c], Isabelle Allaeys[a], Julien Prunier[d], Oumaima Azeggouar Wallen[e], Élizabeth Dumais[e], Clémence Belleannée[b], Arnaud Droit[d], Nicolas Flamand[e,f], Éric Boilard[a,g,h], and Louis Flamand[a,g,h,1]

Affiliations are included on p. 11.

Edited by Barry Coller, The Rockefeller University, New York, NY; received October 15, 2024; accepted January 27, 2025

Platelets, known for maintaining blood balance, also participate in antimicrobial defense. Upon severeacute respiratory syndrome coronavirus 2 (SARS-CoV-2) infection, platelets become hyperactivated, releasing molecules such as cytokines, granule contents, and bioactive lipids. The key effector biolipids produced by platelets include 12-hydroxyeicosatetraenoic acid (12-HETE) and 12-hydroxyeicosatrienoic acid (12-HETrE), produced by 12-lipoxygenase (12-LOX), and prostaglandins and thromboxane, produced by cyclooxygenase-1. While prostaglandin E2 and thromboxane B2 were previously associated with lung inflammation in severe COVID-19, the role of platelet 12-LOX in SARS-CoV-2 infection remains unclear. Using mice deficient for platelets' 12-LOX, we report that SARS-CoV-2 infection resulted in higher lung inflammation characterized by histopathological tissue analysis, increased leukocyte infiltrates, and cytokine production relative to wild-type mice. In addition, distinct platelet and lung transcriptomic changes, including alterations in NOD-like receptor (NLR) family pyrin domain-containing 1 (NLRP1) inflammasome-related gene expression, were observed. Mass spectrometry lipidomic analysis in 12-LOX-deficient-infected mice revealed significant changes in bioactive lipid content, including reduced levels of 12-HETrE that inversely correlated with disease severity. Finally, platelet 12-LOX deficiency was associated with increased morbidity and lower survival rates relative to wild type (WT) mice. Overall, this study highlights the complex interplay between 12-LOX-related lipid metabolism and inflammatory responses during SARS-CoV-2 infection. The findings provide valuable insights into potential therapeutic targets aimed at mitigating severe outcomes, emphasizing the pivotal role of platelet enzymes in the host response to viral infections.

platelet type-12 lipoxygenase | SARS-CoV-2 | 12-HETrE | Inflammation | platelets

Significance

Severe COVID-19 is associated with uncontrolled inflammation, leading to acute respiratory distress. We found that mice deficient in platelets' 12-lipoxygenase (12-LOX) demonstrate exacerbated inflammation and worse outcomes following severe acute respiratory syndrome coronavirus 2 (SARS-CoV-2) infection. One mediator derived from platelet 12-LOX activity, 12-hydroxyeicosatrienoic acid (12-HETrE), was found to negatively correlate with disease severity. Taken together our data unravel a possible role of platelets and possibly 12-HETrE, which is documented as promoting anti-inflammatory effects, in dampening the inflammatory burden of infected mice and pinpoints potential new therapeutic strategies (12-LOX inhibitors or 12-HETrE receptor agonists) to better combat severe COVID-19.

COVID-19 is a viral disease caused by the severe acute respiratory syndrome coronavirus 2 (SARS-CoV-2) (1). SARS-CoV-2 induces lung alveolar and interstitial inflammation, leading to acute respiratory distress syndrome, shock, and multiple organ dysfunction, in the most severe cases (2). The uncontrolled inflammation caused by the disease results in a state of hypercoagulability, and many patients show hemostatic abnormalities that are associated with an increased risk of death (3, 4). Due to the relevance of COVID-19-coagulation abnormalities, the role of platelets and megakaryocytes (MKs) in the pathogenesis of SARS-CoV-2 infection has become a subject of investigation. A hyperactivated and prothrombotic state of platelets has been consistently associated with SARS-CoV-2 infection (5–7). This altered state is accompanied by substantial alterations in the transcriptome and functional changes in platelets that contribute to SARS-CoV-2 pathophysiology by increased platelet–platelet and platelet–leukocyte interactions (5, 8, 9).

Recent studies are elucidating the immunoregulatory role of platelets and MKs, which, in addition to their traditional role in hemostatic and thrombosis regulation, have multiple functions mediating immune functions during infection and inflammation (10–12). Platelets express pattern recognition receptors, Fc receptor, and other types of receptors for recognizing the presence of pathogens (12–14). Platelets can interact with neutrophils, monocytes, or lymphocytes to amplify the immune response or release cytokines and lipid mediators that will affect their activity or other immune cells (6, 15).

Lipid mediators of inflammation (LMI) produced by platelets and other immune cells are important contributors of inflammation, including the resolution and healing process (16). Lipid profiling in the lungs of humans or mice infected with SARS-CoV-2 has indicated substantial LMI modulation, suggesting that infection influences lipid profiles, particularly eicosanoids and docosanoids in humans and mice (17–19). Pulmonary circulation MKs

Author contributions: A.C.d.S.P.A., N.F., É.B., and L.F. designed research; A.C.d.S.P.A., E.L., I.D., L.G., A.G., F.P., G.C.-S., C.Q.-J., I.A., O.A.W., and É.D. performed research; J.P., C.B., and A.D. contributed new reagents/analytic tools; A.C.d.S.P.A., E.L., J.P., N.F., É.B., and L.F. analyzed data; and A.C.d.S.P.A., and L.F. wrote the paper.

The authors declare no competing interest.

This article is a PNAS Direct Submission.

[1]To whom correspondence may be addressed. Email: louis.flamand@crchudequebec.ulaval.ca.

This article contains supporting information online at https://www.pnas.org/lookup/suppl/doi:10.1073/pnas.2420441122/-/DCSupplemental.

Published March 18, 2025.

actively release large quantities of platelets, suggesting that the lungs are a site for platelet biogenesis (20). The contribution of LMIs produced by MKs and platelets in the modulation of the lung lipid signature observed in COVID-19 requires further investigation.

LMIs production in platelets occurs when various stimuli trigger the release of polyunsaturated fatty acids (PUFAs), a process notably involving but not restricted to the group IVA cytosolic phospholipase A2 (cPLA$_2\alpha$) (21). Unesterified PUFAs, such as linoleic acid (LA), arachidonic acid (AA), eicosapentaenoic acid (EPA), docosahexaenoic acid (DHA), and dihomo-gamma-linolenic acid (DGLA), are metabolized predominantly by platelet-type 12-lipoxygenase (12-LOX) and cyclooxygenase 1 (15, 22). 12-LOX has been shown to play an important role in regulating platelet activation (15, 23–25). Indeed, pharmacological inhibition of 12-LOX by the compound ML355 results in a significant attenuation of human thrombin and FcγRIIa-mediated aggregation of human platelets and disrupts thrombus growth and vessel occlusion in vivo (15, 25). Furthermore, individuals with deficient lipoxygenase activities demonstrate reduced platelet activation, while episodes of hemorrhage prevail over thrombosis in 67% of cases (26). Accordingly, experimental models involving *Alox12* (gene coding for platelet 12-LOX) knockout (KO) mice also display impaired thrombus formation, characterized by delayed platelet adhesion, aggregation, and thrombus formation (25, 27). The main platelet 12-LOX-derived oxylipins responsible for modulating platelet functions are 12-hydroxyeicosatetraenoic acid (12-HETE), 12-hydroxyeicosatrienoic acid (12-HETrE), and 12-hydroxyeicosapentaenoic acid (12-HEPE), derived from the substrates AA, DGLA, and EPA, respectively (23).

Despite the identification of these 12-LOX-derived oxylipins in platelets decades ago and progress made in understanding their role in regulating hemostasis, their involvement in the inflammatory response remains incompletely understood. Using *Alox15 KO* mice Pernet etal. (28) reported that a deficiency in neutrophil-derived 12-HETE compromises the self-renewal and maintenance of alveolar macrophages, resulting in increased susceptibility to acute lung injury following SARS-CoV-2 infection (28). Importantly, the roles of platelet 12-LOX activity on pulmonary immunity, was not studied.

Given the evident contribution of platelets to the pathogenesis of COVID-19 and the crucial regulation of 12-LOX in platelet activity, we sought to investigate the significance of the platelet enzyme in SARS-CoV-2 pathogenesis. Utilizing the widely described animal model of SARS-CoV-2 infection (K18-hACE2) (29), we introduced a KO for the platelet 12-LOX enzyme into this model and assessed the impact of this loss on the infection outcome. Overall, our results identify platelet 12-LOX as a beneficial enzyme during SARS-CoV-2 infection whose deficiency is associated with exacerbated inflammation and disease severity.

Methods

Cells and Virus. Vero cells were obtained from the American Type Culture Collection (Manassas, VA) and cultured in Medium 199 (Multicell Wisent Inc., St-Bruno, QC, Canada) supplemented with 10% fetal bovine serum (FBS) and 5 μg/mL of Plasmocin®. A549-hACE2 cells were purchased from BEI Resources and were cultured in Dulbecco's Modified Eagle Medium (Corning Cellgro) with 10% FBS, 10 mM N-[2-Hydroxyethyl]piperazine-N′-[2-ethanesulfonic acid] (HEPES) pH 7.2, 1% v/V nonessential amino acids, and 5 μL/mL Plasmocin. To maintain hACE2 expression, 50 μg/mL of blasticidin (ant-bl-1, Invivogen) was added every second passage (30). Cell lines were grown at 37 °C with 5% CO_2. The SARS-CoV-2 Delta strain used in mice infections was obtained from the National Microbiology Laboratory (Winnipeg, Manitoba). The virus was propagated on Vero cells. The infectious titer of the viral preparation was 1.8×10^6 Tissue Culture Infectious Dose 50/mL ($TCID_{50}$/mL). Experimentation with infectious SARS-CoV-2 virus propagated in A549-hACE2 cells was conducted in a biosafety level 3 confinement (BSL-3) facility. Influenza A/PR8 H1N1 virus was obtained from the American Type Culture Collection (31).

Platelet activation experiments were performed with SARS-CoV-2 [strain Laboratoire de Santé Publique du Québec (LSPQ), B1 lineage] obtained from the LSPQ (Sainte-Anne-de-Bellevue, QC, Canada) propagated in A549-hACE2 cells or conditioned media obtained from noninfected A549-hACE2 cells as previously described 7.

Mouse Strain. Animal experimental procedures were carried out with mixed groups (males and females) of mice aged 8 wk under BSL-3 for SARS-CoV-2 infection and under BSL-2 for Influenza infections. Guidelines of the Canadian Council on Animal Care were followed in a protocol approved by the Animal Welfare Committee at Laval University (Project: 2020-594). cPLA$_2\alpha$ KO mice (*Pla2g4a* KO) (B6.129S4-Pla2g4atm1Jvb), were kindly provided by Michael H. Gelb, University of Washington, and backcrossed into pure C57Bl6/J background (32). K18-ACE2 mice (B6.Cg-Tg 2Prlmn/J, stock no. 3034860), platelet *Alox12* KO mice (*Alox12* KO) (B6/J-Alox12tm1Fun/J, stock no.004042), and Thromboxane synthase 1 (*Txas*) KO mice (B6.129P2-Tbxas1tm1Swl/J) were purchased from the Jackson Laboratories and were backcrossed into pure C57Bl6/J background (Bar Harbor, ME). Tryptophan hydroxylase 1 (Tph1) KO mice were generously provided by Francine Côté (33). K18-ACE2::*Pla2g4a*−/−, K18-ACE2::*Alox12*−/− K18-ACE2::*Alox12*−/−, K18-ACE2::*Txas*−/−, and K18-ACE2::*Tph1*−/− mice were maintained fully backcrossed in the C57BL/6 background and generated by crossing K18-ACE2 mice with *Pla2g4a*−/−, *Alox12*−/−, *Txas*−/−, and *Tph*1−/− mice with genotyping performed as per Jackson Laboratory recommendations. Mice were housed in individually ventilated cages at 24 °C on a 12-h light/12-h dark cycle, receiving ad libitum access to water and food.

Mice Infection. Viral infection of 8 to 10-wk-old mice was performed intranasally after anesthesia with isoflurane. For this, 25 μL of sterile saline solution containing 500 $TCID_{50}$ of the SARS-CoV-2 Delta variant or H1N1 virus was administered to each animal. In the noninfected control groups, only saline was administered. After infection, the mice were monitored for up to 14 d postinoculation. Mouse body weight was recorded daily.

Sample Processing. On days 1, 3, and 5, mice (n = 5/group) were killed by exsanguination under isoflurane anesthesia. Lobes from the right lung were homogenized in PBS using the Omni Bead Ruptor Bead Mill homogenizer (Kennesaw, GA) and used for viral load and cytokine/ LMI determinations. The left superior lobes of the lungs were preserved in 10% neutral buffered formalin for 24 h before being embedded in paraffin for histological examination as previously described (34). The lung's left inferior lobe was used for RNA extraction. Blood samples were collected by cardiac puncture.

Determination of the Viral Titer. Vero cells were plated in a 96-well plate (2×10^4/well) and infected with 200 μL of serially diluted viral preparations of lung homogenates in M199 media supplemented with 10 mM HEPES pH 7.2, 1 mM of sodium pyruvate, 2.5 g/L of glucose, 5 μg/mL Plasmocin®, and 2% FBS. Three days postinfection plates were analyzed for signs of cytopathic effects using an EVOS M5000 microscope (ThermoFisher Scientific, Waltham, MA), and the viral titer was determined using the Karber method (30, 35).

Hematological Evaluation. The number of circulating platelets and leukocytes was measured in blood samples by flow cytometry. Blood samples were collected by cardiac puncture (600 μL in a 420 μL citrate anticoagulant solution and Tyrode's buffer -pH 6). Whole blood was first incubated with mouse BD FC Block (5 mg/mL, catalog no. 553141; BD Pharmingen) and then with the fluorescent-labeled monoclonal antibodies: CD41-APC (6 μg/mL, cat.no: 561425, BD-Bioscience), activated integrin αIIbβ3*-PE (1:33, cat.no: 340507, BD-Bioscience) and CD62P-FITC (20 μg/mL, cat.no: 550888, BD-Bioscience); CD3-BV421 (2.8 μg/mL, cat. no: 564008, BD-Bioscience), Ly6G-BV421 (2.8 μg/mL, catalog no. 562737; BD-Bioscience), CD45-BV421 (2.8 μg/mL, catalog no. 563890; BD-Bioscience), CD4-PE (3.2 μg/mL, catalog no. 553049; BD-Bioscience), CD8-APC (6 μg/mL, catalog no.553035; BD-Bioscience), CD3-APC (7.2 μg/mL, cat.no: 100236, BD-Biolegend), B220-FITC (7.2 μg/mL, cat.no: 557669, BD-Bioscience). After 20 min incubation at 37 °C, samples were fixed with 450 μL paraformaldehyde (1%) solution. The acquisition was carried out in a BD fluorescence activated cell sorter (FACS) Canto II cell analyzer and for platelets, FACS Canto-II was combined with a forward scatter coupled to a photomultiplier tube "small particles option"

flow cytometer (BD Biosciences, CA). All acquisitions were analyzed using FlowJo software (Tree Star, Ashland, OR). Leukocytes and platelets were quantified by addition of a known concentration of Silica beads 15 μm and 2 μm, respectively (Kisker Biotech, Germany), as previously described (6, 7).

Platelet Isolation. Mouse blood was collected in citrate-containing tubes and centrifuged for 3 min at 500 g room temperature (RT). Supernatant were transferred to new tubes and centrifuged for 2 min at 300 g, RT to obtain platelet-rich plasma (PRP). After a two-step centrifugation (2 × 2,500 g, 15 min, RT), PRP were transferred to a new tube and 20% of acid-citrate-dextrose (ACD) and Ethylenediaminetetraacetic acid (EDTA) (final concentration 10 mM) were added. After, an additional centrifugation was done (5 min at 1,100 g, RT), and the pellet was resuspended in 100 μL Tyrode's buffer (pH 6.5). Seven hundred microliters of Tyrode's buffer (pH 7.4), 200 μL ACD and EDTA (final concentration 10 mM) were added, and the tube was centrifuged for 5 min at 1,300 g, RT. The pellet was recovered in Tyrode's buffer pH 7.4. To obtain purified platelet populations for RNA analysis LS columns (Miltenyi Biotec®) and magnetic cell sorting separation (MACS) MicroBeads (CD45 Microbeads mouse cat. no: 130-052-301 and Anti-TER-119 Miltenyi Biotec® cat.no: 130-049-901) were used for depletion of CD45 and TER119 positive cells. The purity of platelet suspensions acquired after magnetic isolation was assessed by Flow cytometry. Three μL of platelets suspension was transferred to 22 μL staining solution containing antibodies for mouse CD41 (1 μL, cat.no: 133914, Biolegend), CD45-BV421 (2.8 μg/mL, catalog no. 563890; BD-Bioscience), TER-119 (1 μL, cat.no: 557909, BD-Bioscience), and CD62P (0.5 μL, cat.no: 553744, BD-Bioscience). After 20 min of incubation, 250 μL of paraformaldehyde-solution (PFA, 1% in PBS) was added, and samples were analyzed in a BD FACS Canto II (BD Biosciences, CA).

Washed human platelets were obtained from venous blood collected from healthy donors (four women adult donors) into a citrate anticoagulant solution using the same protocol described in ref. 7. Informed consent was obtained from all participants. This study was approved by the ethics committee (Centre Hospitalier Universitaire de Québec) (Project: 2021-5303).

Platelet Activation assay. Human platelet-free plasma was incubated in Tyrode's buffer (pH 7.4, 10 mM $CaCl_2$) with stimuli (supernatant of A549-hACE2 cells infected with SARS-CoV-2 or conditioned media) for 60 min in a volume of 20 μL. Then, 20 μL of twice-washed human platelets (200 × 10^6/mL) were added, resulting in a final reaction volume of 40 μL. Platelet activation was assessed after 60 min by transferring 3 μL of the final reaction mixture to 22 μL of staining solution containing antibodies for human CD41 (0.3 μL, cat. no: 561425, BD-Bioscience), activated integrin αIIbβ3* (2 μL, cat. no: 340507, BD-Bioscience), and CD62P (1 μL, cat. no: 550888, BD-Bioscience) in Tyrode's buffer (pH 7.4). After 20 min of incubation, 250 μL of PFA solution (1% in PBS) was added, and the samples were fixed for 20 min before analysis by flow cytometry. The frequency (%) of αIIbβ3*+CD62P+ platelets for all platelets was quantified. Twice-washed murine platelets (200 × 10^6/mL) were incubated in Tyrode's buffer (pH 7.4, 10 mM $CaCl_2$) with stimuli (Thrombin 1U/mL or vehicle) for 15 min in a total volume of 200 μL. After this, ACD and EDTA (140 mM) were added to the samples, and they were centrifuged at 1,300 g for 5 min. The lipids present in the supernatant were analyzed by liquid chromatography–tandem mass spectrometry (LC–MS/MS). CXCL4 was measured using mouse CXCL4 DuoSet enzyme-linkedimmunosorbent assay (ELISA) (R&D System, #DY595) according to the manufacturer's protocol.

D-Dimer Measurements. Plasma samples from mock-infected and SARS-CoV-2-infected mice were analyzed for the presence of D-Dimers by the ELISA according to the manufacturer's guidelines (Biomatik Corporation, Kitchener, ON, Canada).

Histopathology. Lung tissues embedded in paraffin were sectioned into 5-mm thickness slices as previously described (34), stained with Carstairs' stain reagents (36), and examined under light microscopy. The assessment of inflammation-related damage in mouse lungs was performed by a pathologist (C.Q.-J.) who was unaware of the experimental conditions, employing a scoring system encompassing i) airway inflammation (up to four points), ii) vascular inflammation (up to four points), iii) parenchyma inflammation (up to five points), and iv) general neutrophil infiltration (up to five points) (37).

Immunofluorescence and Confocal Microscopy. Immunofluorescence assays were conducted to identify the pan-T lymphocyte marker CD3 (Rat anti-CD3 MA5-16622, clone CD3-12, Invitrogen), the neutrophil marker Ly6G-C (Rat anti-Ly6G/6C, Cat: 553123, clone RB6-8C, BD Biosciences), and the macrophage marker F4/80 (Cat: 123101, clone BM8, Biolegend). Goat anti-rat Alexa-AF647 (Cat: A48265, Invitrogen) was used in 5-μm lung sections embedded in paraffin of mice at 3 and 5 dpi, following established methods (30, 34). Cell nuclei were counterstained with DAPI (1 μg/mL) for 5 min. The sections were examined using a Zeiss LSM 880 confocal laser scanning microscope, equipped with lasers and filters suitable for detecting the fluorophores. Images were obtained using a 20× objective (Zeiss, Apochromat).

Multiplex Cytokine Quantification. Mouse lung homogenate in PBS (200 μL) was subjected to a viral inactivation protocol, adding triton at a final concentration of 1% v/v. After centrifugation (14,000 g, 15 min, 4 °C), the supernatant was collected and submitted to a dosage of Cytokines using a ProcartaPlexTM Mouse Mix & Match Panels kit (Invitrogen Waltham, MA) on the Bio-Plex 200 (Bio-Rad Laboratories Ltd.). The total protein content of lung homogenates was quantified using the BCA Protein Assay kit (Thermo Fisher Scientific, Waltham, MA) and employed for normalizing cytokine concentrations (pg of cytokines/mg of total protein).

RNA Extraction and RNASeq Analysis. RNA from lungs of mice and from isolated platelets were extracted using the Bead Mill Tissue RNA Purification Kit and the Omni Bead Ruptor Bead Mill homogenizer (Kennesaw, GA). RNA libraries were generated using the New England Biolab (NEB) Next Ultra II directional RNA library and NEBNext ribosomal RNA (rRNA) Depletion kits (New England Biolab, Ipswich, MA) and analyzed using the NovoSeq 6000 sequencer from Illumina (Vancouver, BC, Canada). This sequencing procedure yielded a total of 703 × 10^6 reads, each presenting a length of 100 bp. Sequencing quality was assessed for all reads using fastqc0.11.7, and low-quality sequencing as well as remaining adaptor nucleotides were discarded using trimmomatic 0.36 which resulted in a total of 623.2 × 10^6 reads of 100 bp on average. The gene expression levels were assessed using the pseudoalignment approach implemented in Kallisto0.46.1 (38). We applied this method using cleaned reads and a composite reference transcriptome including both murine and SARS-Cov-2 coding sequences. Normalizations and statistical tests for differential expressions between time points were performed using the "DESeq2" R-package (39). Principal component analysis was conducted utilizing normalized gene expression levels and the R statistical software (40). Genes were considered differentially expressed among groups when *P*-adjusted value <0.05, along with Log2 fold change (≤−1 and ≥1, lung samples; ≤−0.5 and ≥0.5, platelets).

LMI Analysis. LMIs were measured in lung homogenates and supernatants of human washed platelets using LC–MS/MS and established protocols (17, 18, 41). Lung homogenates (200 μL, protein concentration ranging from 2 to 4 mg/mL) were first diluted to 500 μL with cold (4 °C) Tris-HCl buffer (pH 7.40, 50 mM). Lipids from the diluted samples were next extracted from the diluted samples. Water and solvents were LC–MS grade except $CHCl_3$ (HPLC Plus, 99.9% pure). In brief, the above samples were mixed with 500 μL of MeOH containing 0.1 M AcOH and the deuterated internal standards. One mL of $CHCl_3$ was then added to each sample, vortexed for 30 s, and centrifuged at 3,000 × *g* for 5 min. The $CHCl_3$ fraction was harvested and the samples were exposed to $CHCl_3$ twice again for a total addition of 3 mL $CHCl_3$. The organic phases were pooled and evaporated using a speed-vac evaporator and then suspended in 60 μL of mobile phase containing 50% of solvent A (water + 1 mM ammonium acetate + 0.05% acetic acid) and 50% of solvent B (acetonitrile/water (95/5) + 1 mM ammonium acetate + 0.05% acetic acid]. 40 μL of each sample were injected onto an high performance liquid chromatography (HPLC) column (Kinetex C8, 150 × 2.1 mm, 2.6 μm; Phenomenex) and eluted at a flow rate of 0.4 mL/min using a discontinuous gradient of solvent A and solvent B (from 10% solvent B to 75% in 20 min, from 75 to 95% in 10 s, and held for 5 min at 95% followed by re-equilibration to 10% B during 3 min. Quantification of lipid mediators was carried out by HPLC interfaced with a Shimadzu 8050 triple quadrupole mass spectrometer and using multiple reaction monitoring in negative ion mode (with the exception of prostaglandins-glycerol and prostamides in positive mode) for the compounds and their deuterated homologs or a surrogate (*SI Appendix*, Table S1). Finally, LC–MS/MS analyses were done in a blind fashion, with coded samples, for which the analyst was not aware of the experimental conditions. Measurements of 12(S)-HETE were also made using the ELISA in the plasma of mice throughout the infection, employing the 12(S)-HETE ELISA Kit (Cayman Chemical). Plasma samples were collected after a two-step centrifugation (2,500 g, 15 min, RT). Differential production of lipid sets in

the KO versus WT groups for each time point was analyzed using mass spectrometry results, with the aim of identifying statistically significant Log 2-fold changes through MetaboAnalyst One-factor Statistical Analysis tools (42, 43).

Statistical Analyses. Prism 8.2.1 software (GraphPad) was employed for statistical analysis. Normality was assessed using the Anderson–Darling test. Unless otherwise stated, Student's *t* test or Mann–Whitney *U* test was utilized for comparing two groups and ordinary one-way ANOVA with Fisher's least significant difference (LSD) post hoc test or Kruskal–Wallis test with Dunn's post hoc test for multiple groups. Survival rates across groups were analyzed through Kaplan–Meier survival analysis. Additionally, body weight changes induced by SARS-CoV-2 were compared among groups using two-way repeated measures ANOVA. Individual values represent the number of samples, and data are expressed as the mean ± SEM. Differences with a *P* value of less than 0.05 were deemed statistically significant.

Results

SARS-CoV-2 Activates Platelet-Type 12-LOX. Platelet hyperreactivity and excessive inflammation are some of the main features observed during severe COVID-19. Two main class of soluble mediators cause inflammation: cytokines and LMI. Abundant literature exists on cytokines associated with severe COVID-19 (44, 45) but much fewer studies have assessed the contribution of LMI during disease. To gain a deeper understanding of platelet responses during SARS-CoV-2 infection, we initiated an investigation to determine whether the virus itself would activate key platelet enzymes associated with the production of LMIs. Isolated human platelets were incubated in the presence of supernatants derived from SARS-CoV-2-infected A549-hACE2 cells, as previously described by Puhm et al. (7), and analyzed for the expression of P-selectin and the activated conformation of integrins αIIbβ3 (Fig. 1*A*). Our analyses showed increased platelet activation in the presence of SARS-CoV-2 (Fig. 1*B*), corroborating previous findings (7). The corresponding supernatants were subjected to mass spectrometry to identify and quantify the major lipids produced by platelets in response to SARS-CoV-2 exposure. Platelets responded to SARS-CoV-2 by releasing a variety of metabolites. Of these, the 12-LOX metabolite 12-HETE was the one produced in the largest quantity among those with significant increases (Fig. 1*C*). Other 12-LOX metabolites, including 12-HETrE and 12-HEPE, were also produced at significantly higher levels following exposure to the virus. COX-derived metabolites (PGE2 and TXB_2) were produced at higher levels in response to the virus but these increased failed to reach statistical significance. These findings suggest that AA is preferentially processed by 12-LOX in platelets under these conditions.

cPLA$_2$α Deficiency Exacerbates Inflammation during SARS-CoV-2 Infection. To assess the significance of the LOX and COX lipid production pathways on SARS-CoV-2 pathogenesis, we compared infection in *Pla2g4a* KO and WT mice. The *Pla2g4a* deficiency was introduced in the background of SARS-CoV-2 susceptible K18-h*ACE2* transgenic mice to generate K18-*ACE2 Pla2g4a* KO mice. Nine-week-old WT (K18-*ACE2*) and *Pla2g4a* KO (K18-*ACE2 Pla2g4a*−/−) mice of both sexes were infected intranasally with 500 $TCID_{50}$ of SARS-CoV-2. *Pla2g4a* KO mice experienced lower survival (*SI Appendix*, Fig. S1*A*) and greater weight losses (*SI Appendix*, Fig. S1*B*) but these results did not reach statistical significance. Lung viral loads (*SI Appendix*, Fig. S1*C*) were similar between *Pla2g4a KO* and WT mice. Relative to WT mice, *Pla2g4a KO* mice did however exhibit significantly higher pulmonary inflammatory scores (Fig. 1 *D* and *E*) with an increase in proinflammatory cytokines such as CXCL-1, CCL-2, CXCL-9, and IFN-γ in lung homogenates during infection (Fig. 1*F*). The lipid mediators in the lungs of the *Pla2g4a KO* mice showed significant reductions in the release of EPA and PGE3 (*SI Appendix*, Fig. S1 *G* and *N*). Levels of 12-HEPE, also derived from EPA, followed a similar trend but the decrease observed in *Pla2g4a KO mice* failed to reach statistical significance (*SI Appendix*, Fig. S1*J*).

Loss of Platelet 12-LOX Alters the Lipidome. As 12-LOX is one main platelet enzyme downstream of cPLA$_2$α, with critical relevance to platelet activation that may be associated with the increased inflammation observed in *Pla2g4a* KO animals, we next generated K18-hACE2 mice deficient for platelet 12-LOX. As expected, and in contrast to platelets from WT mice, isolated platelets from 12-LOX-deficient mice failed to biosynthesize 12-HETE, 12-HEPE, and 12-HETrE when treated with thrombin. In contrast, TXB2 biosynthesis was slightly increased in thrombin-stimulated KO versus WT mouse platelets (Fig. 2*A*). We next examined the impact of platelet *Alox12* deletion on the production of bioactive lipids during SARS-CoV-2 infection. Fig. 2*B* depicts the main lipid precursors produced by PLA$_2$s, and the enzymes catalyzing their conversion into bioactive lipids. In WT mice, plasma concentrations of 12(S)-HETE varied between 100 to 150 pg/mL and remained similar between mock and SARS-CoV-2-infected mice (Fig. 2*C*). Relative to WT mice, *Alox12* KO mice had 12(S)-HETE levels that were considerably less (10 to 35 pg/mL), indicating that platelet 12-LOX is a major contributor of circulating 12(S)-HETE (Fig. 2*C*). It should be noted that during plasma preparation, the extracellular vesicles that can be a source of 12(S)-HETE (46), were not removed. Residual levels of 12(S)-HETE in the plasma of *Alox12* KO mice might be attributable to activity by other enzymes like 12/15- LOX or cytochrome P450 in different cellular types (47–49).

In the lungs, the levels of AA, DHA, and EPA increased markedly, in both *Alox12* KO and WT mice as infection progressed (Fig. 2 *D*–*G*). The biosynthesis of 12-HETE and 12-HETrE metabolites was however severely compromised in the *ALOX12* KO mice (Fig. 2 *H* and *I*). The biosynthesis of Maresin 2 (Mar2) and Protectin Dx (PDx), two DHA-derived mediators with documented anti-inflammatory effects, were also found to be reduced in the lungs of *Alox12* KO mice at all times postinfection (Fig. 2 *J* and *K*), in contrast to the WT group, where Mar2 and PDx levels correlated with those of its precursor DHA (Fig. 2*F*). Of note, the levels of Mar2 and PDx were low and close to the limit of quantification. Acknowledging the challenges in accurately identifying SPMs in samples by LC–MS/MS, as demonstrated in previous studies (50), we have provided examples of raw and unprocessed LC–MS/MS data in *SI Appendix*, Fig. S2 confirming that the obtained peaks were appropriately interpreted. Noteworthy, while we also analyzed the levels of Mar1 and RVD1-5, those mediators were not detected in our samples.

Levels of 15(S)-HETE in *Alox12* KO mice were also less than WT mice (Fig. 2*L*). AA-derived metabolites produced by the COX enzyme—PGE_2, PGF_2a, PGD_2, and TXB_2 were consistently increased throughout the infection in both groups of mice (Fig. 2 *M*–*P*). Relative to WT mice, PGE_2, $PGF_{2α}$, PGD_2, and TXA_2, levels in *Alox12* KO mice were significantly lower on day 1 postinfection. Unexpectedly, considering that LTB4 is a 5-LOX-derived metabolite, *Alox12 KO* mice produced significantly less LTB4 than WT mice throughout the course of infection (Fig. 2*Q*).

Analysis of the log 2-fold change in lipid production in the lungs between the *Alox12* KO and WT groups revealed that in the mock-infected groups, there was no statistically significant difference (Fig. 2*R*). In the absence of an infection stimulus, the variations in lipid production are insufficient to influence any

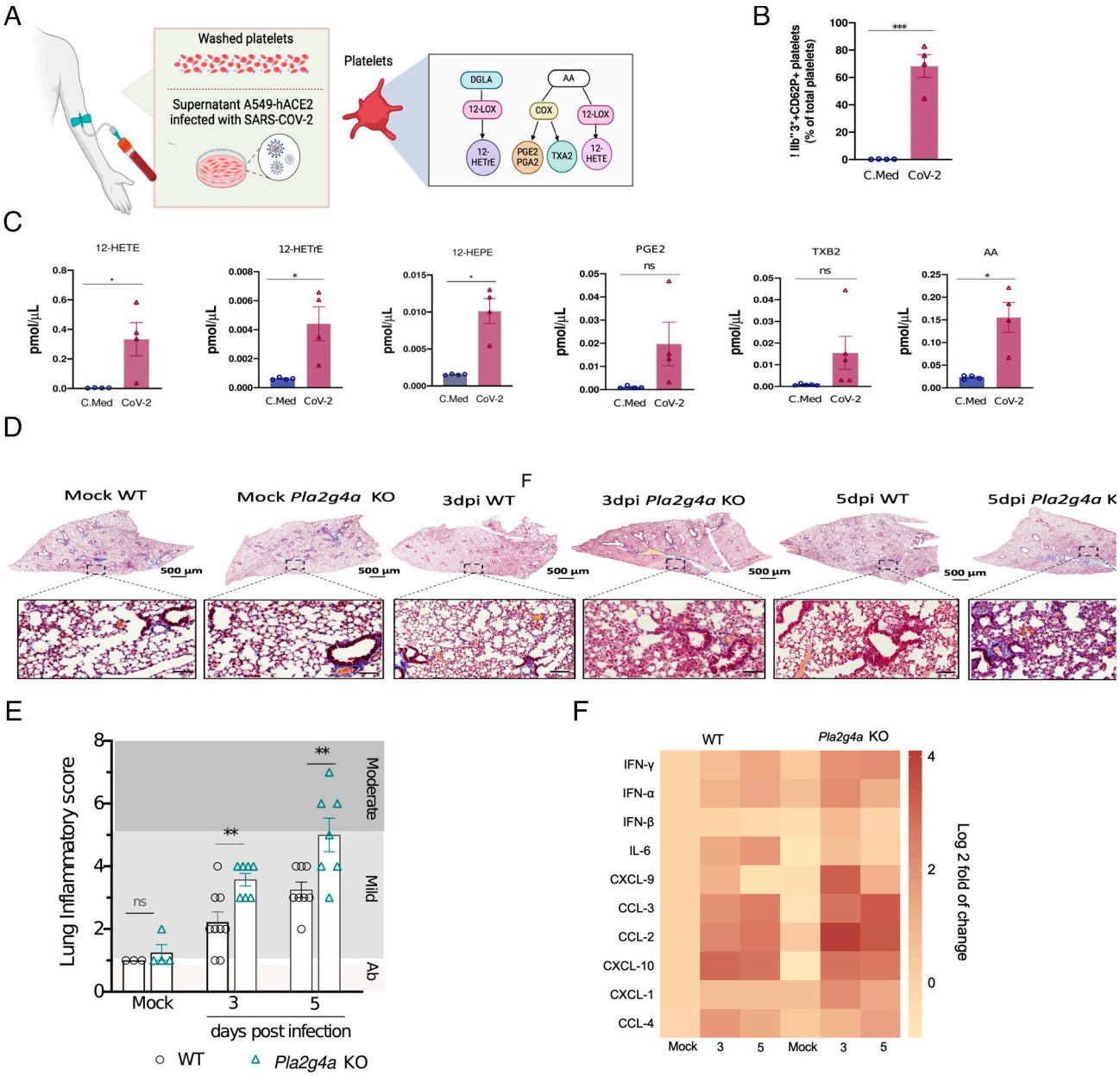

Fig. 1. Activation of the cPLA$_2$α downstream pathway during SARS-CoV-2 infection. (*A*) Study design. Human washed platelet responses to A549-hACE2 cell culture conditioned media from mock-infected (C.Med) or infected SARS-CoV-2 (CoV-2) (cell culture supernatant obtained after 4 d of culture and treatment with b-propiolactone to inactivate the virus). (*B*) Platelets from four donors were stimulated for 60 min, labeled, fixed, and analyzed by flow cytometry. (*C*) Lipid mediators, 12-HETE;12-HETrE; 12-HEPE; PGE$_2$; TXB$_2$ produced by human platelet in response to SARS-CoV-2 exposure were analyzed by LC–MS/MS. (*D*) Images of mouse lung sections, stained using the Carstairs technique, highlighting the general histological changes across WT and *Pla2g4a KO*-infected mice with 500 TCID$_{50}$ of SARS-CoV-2/mouse (n = 4 to 8). (*E*) Assessment of lung inflammation scores among WT and *Pla2g4a* KO groups. (*F*) Heatmap of cytokine concentrations determined in lung homogenates through multiplex cytokines quantification (pg/mg of lung). Results are expressed as fold (log2) relative to WT-mock-infected mice (n = 8 to 10/group). Statistical differences were analyzed by Student's *t* test or ordinary one-way ANOVA plus Fisher's LSD test. Mann–Whitney test or Kruskal–Wallis plus Dunn's posttest were carried out for nonparametric comparisons. ns: nonstatistically significant. (n = 5) *$P < 0.05$; **$P < 0.005$; ****$P < 0.0001$.

metabolic pathways significantly. However, particularly on the first and 5th day postinfection, several lipid metabolites demonstrated a significant reduction in production in the KO group (Fig. 2*R*). The most prominent reductions were observed in those dependent on 12-LOX for their synthesis, notably 12-HETE, 12-HETrE, 12-KETE, and 12-HEPE (24). These findings suggest that alterations in the lipidome induced by platelet *Alox12* KO in infected mice modulate the activation of distinct metabolic pathways in the lungs compared to the WT group.

Transcriptomic Alterations in Lungs of *Alox12*-Deficient Mice. Considering that LMI influences cellular functions in many ways and that 12-LOX deficiency alters the mouse lipidome, we conducted lung RNA-sequencing analyses in both WT and *Alox12* KO mice groups to unveil RNA-level differences attributed to the absence of platelet 12-LOX enzyme. On average, 10,571 protein-coding genes were identified across the experimental groups. As anticipated, principal component analysis revealed a distinct separation between mock-infected and SARS-CoV-2-infected mice (18), irrespective of their genotype (Fig. 3*A*). Notably, comparisons between WT and *Alox12* KO mice suggested that gene signatures exhibited subtle differences between genotypes with the greatest variations observed on day 3 postinfection. (Fig. 3*A*). This underscores the notion that the infection itself, rather than *Alox12* KO, triggers pronounced alterations in the transcriptome landscape of the lung.

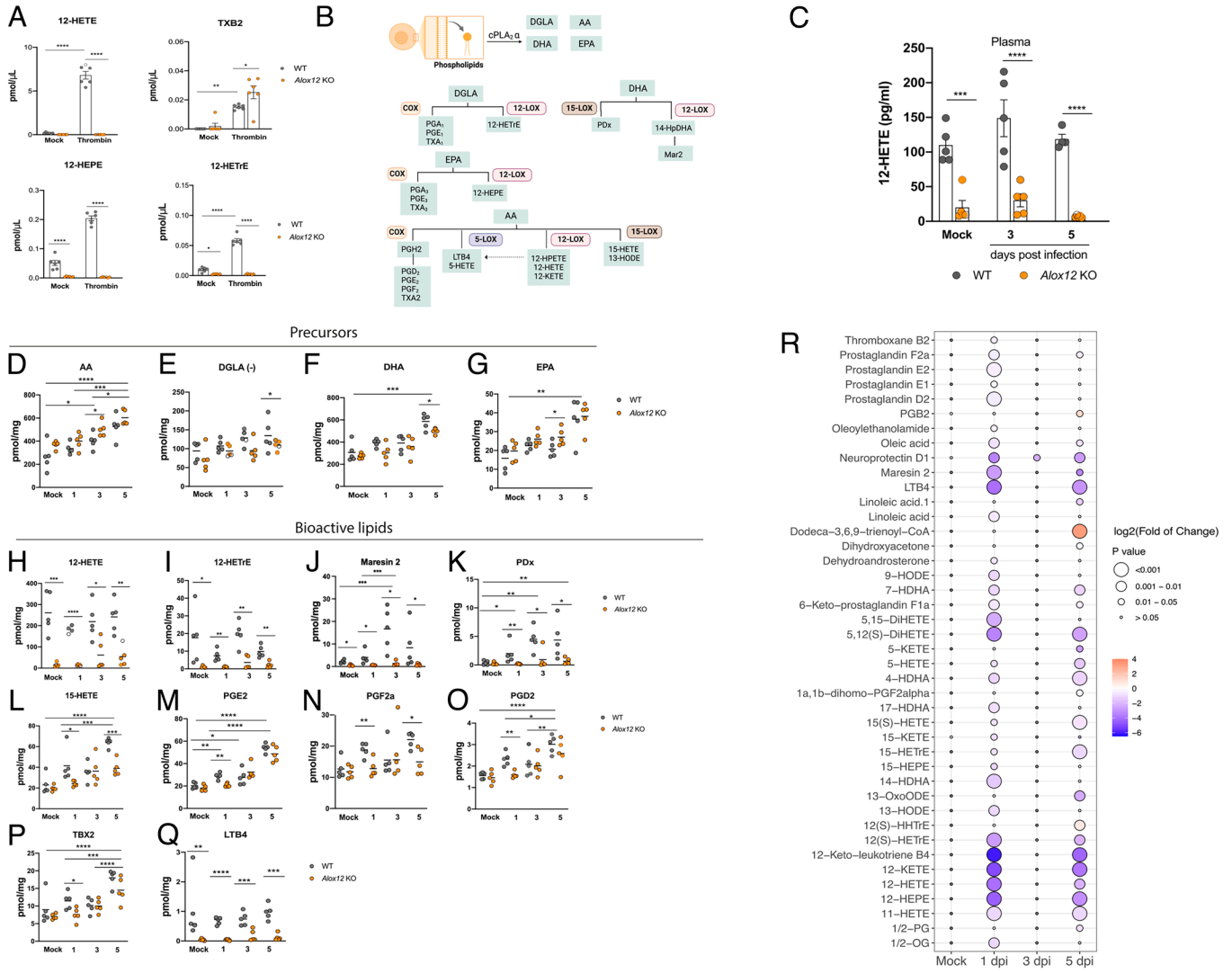

Fig. 2. Modulation of the LMI signature by 12-LOX activity in the lungs of SARS-CoV-2-infected mice. (*A*) 12S-HETE, TXB2, 12-HEPE, and 12-HETrE dosages (pmol/mL) by LC–MS/MS in supernatants of mouse washed platelets stimulated with thrombin (1U/mL), or vehicle (Mock) for 15 min. (*B*) LMI biosynthetic pathways (*C*) 12(S)-HETE ELISA measurements (pg/mL) in plasma on Mock, 3 and 5 d postinfection. (*D*–*Q*) Individual graphs of the main LMIs (pmol/mg of lung tissue) that showed greater modulation with the loss of 12-LOX. (*R*) Dot plot with Log2 Fold change KO versus WT groups of the main LMI dosed over the course of infection. Lung LMI were analyzed by MetaboAnalyst 5.0. Statistical differences were analyzed by ordinary one-way ANOVA plus Fisher's LSD test and Kruskal–Wallis test with Dunn's posttest for nonparametric comparisons. ns: nonstatistically significant. (n = 5) *$P < 0.05$; **$P < 0.005$; ****$P < 0.0001$.

To comprehend the modulation of LMI signatures in the lungs described above, we investigated transcriptional expression of key enzymes involved in their production. Phospholipase A2 genes (*Pla2g4a*, *Pla2g4c*, and *Pla2g7*) and prostaglandin synthase genes (*Ptgs1* and *Ptgs2*) were upregulated on days 3 and 5 postinfection in WT and the *Alox12 KO* groups, correlating with the elevation of these lipids throughout the infection (*SI Appendix*, Fig. S3).

Gene ontology analyses revealed differential expression of genes associated with lipoxygenase metabolism, the inflammasome complex, and the antiviral immune response in both the mock group and at 3 and 5 d postinfection when comparing the WT and *Alox12* KO groups (Fig. 3 *B*–*D*). Upon examining the differentially expressed genes (DEGs) in WT vs. KO comparisons at each postinfection time point, it was observed that three DEGs, *Alox12*, *Nlrp1a,* and *Nlrp1b*, displayed differential expression from the mock stage to 5 d postinfection (Fig. 3*E*). This observation suggests that the unique expression of these genes is not linked to infection but rather attributed to the *Alox12* KO.

Among the genes related to the inflammasome pathway, the genes *Nlrp1a* and *Nlr1b* exhibited significantly downregulated and upregulated expression respectively, in the KO groups (Fig. 3*F*). These genes encode proteins predicted to be part of the NLRP1 inflammasome complex, which functions as a sensor for various pathogen-encoded activities (51). The modulation of gene expression in the inflammasome complex in the lungs of KO mice may result in a distinct response to SARS-CoV-2 infection in these KO animals.

To better understand the modulation of gene expression observed in the lungs of mice, we also assessed gene expression in the washed platelets of these mice by RNAseq. Out of 22,018 annotated mouse protein-coding genes, 13,672 exhibited positive hits. When comparing the DEGs between the uninfected WT and *Alox12* KO groups, we observed 14 downregulated genes involved in hemoglobin and oxygen homeostasis, while two upregulated genes were associated with the Rho guanosine triphosphate (GTP)ase activation pathway as highlighted in the volcano plot (Fig. 3*G*). The gene ontology of these genes revealed enrichment, primarily in the pathways of iron homeostasis signaling and erythrocytes taking up oxygen and releasing carbon dioxide (Fig. 3*H*). Although we employed Anti-TER-119 depletion to remove TER-119 positive cells, residual red blood cells (<0.01%) are still present in our samples, which could account for the differential expression of erythrocyte markers

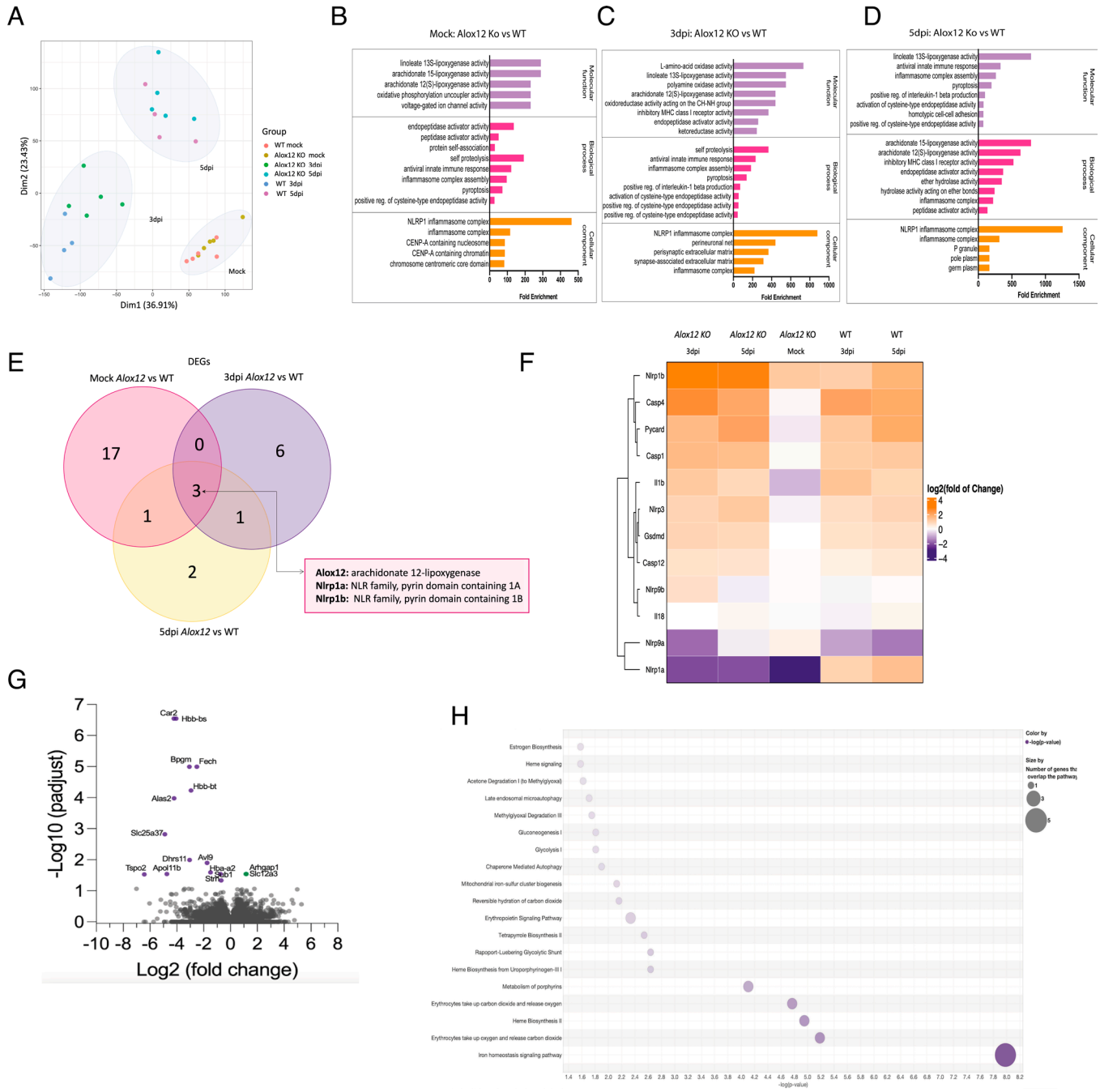

Fig. 3. Lung and platelet transcriptomes during infection of WT and *Alox12*. RNA isolated from the lungs and platelets of mock and SARS-CoV-2-infected mice (n = 4 to 5) underwent RNA sequencing. (*A*) Principal component analysis of 27 lung samples based on normalized gene expression levels. (*B–D*) Gene Ontology enrichment analysis of molecular function, biological processes, and cellular component enriched in lung samples, comparing mice on day 3 and day 5 postinfection with mock-infected mice performed by Shiny GO 0.80 graphical gene-set enrichment tool. (*E*) Venn diagram illustrating the number of DEGs shared among or exclusive to each infected group compared to mock-infected mice. (*F*) Heat map representation of genes encoding the main inflammasome complex genes at 3 and 5 d postinfection normalized by the WT-mock-infected mice (n = 4 to 5). (*G*) Volcano plots illustrating differentially expressed genes (DEGs) in platelet samples of WT and Alox12 KO mock-infected mice. The numbers in the *Left* and *Right* sections of the volcano plots indicate the total downregulated and upregulated genes, respectively. (*H*) Gene Ontology pathway analysis (IPA software, QIAGEN) showing the most enhanced pathway.

such as Hbb-bs, Hbb-bt, Alas 2, and Hba-a2 (52). In the infected groups, we identified only a few DEGs when comparing WT and *Alox12* KO, insufficient for Gene Ontology analysis. Interestingly, one of the limited DEGs observed in the WT and *Alox12* KO analysis at 5 dpi is the *Nrlp1* gene, exhibiting a log2FoldChange of 7.6200869 and an adjusted *P*-value of 0.04.

Combined RNAseq analyses revealed subtle differences in platelet RNA analysis, but significant modulations in pathways related to the recognition and assembly of inflammatory responses to pathogens in the lungs. Given the lungs' role as the primary site for SARS-CoV-2 replication, we consider it imperative to evaluate how these alterations impact the response to infection by this virus in KO mice.

12-LOX Enzyme Modulates Lung Inflammation during SARS-CoV-2 Infection in Mice. To gain a deeper understanding of the impact of 12-LOX on the infection, we further characterized the infection in *Alox12* KO animals. After intranasal infection, WT mice experienced significant weight loss, beginning on the 5th day postinfection (Fig. 4*A*). *Alox12* KO mice displayed significantly

greater weight loss on days 6 ($P < 0.001$), 7 ($P < 0.001$), and 8 ($P = 0.0039$) postinfection compared to WT mice (Fig. 4*A*). Seventy-one percent of WT mice progressed to a moribund state by 8 dpi necessitating killing while 95% of *Alox12* KO mice ($P = 0.0064$) reached end points necessitating killing (Fig. 4*B*). No notable differences in disease manifestation based on sex were observed. Intranasal administration of a lower dose (250 $TCID_{50}$) yielded similar results (*SI Appendix*, Fig. S4 *A* and *B*).

We observed that proinflammatory cytokines, such as CXCL-9, CCL-2, CCL-3, CXCL-10, CXCL-1, and IL-6, were present at greater concentrations in the lungs of *Alox12* KO mice on day 3 postinfection relative to WT infected mice (Fig. 3*C*). Such cytokines were previously reported to account for disease severity (29, 53). The heightened inflammation cannot be attributed to higher viral replication in the lungs of *Alox12* KO mice, as infectious viral titers on days 1, 3, and 5 postinfection were like those of WT mice (*SI Appendix*, Fig. S4*C*).

We also investigated the impact of *Alox12* KO on platelet counts and activity by evaluating the expression of aIIbb3/CD62P activation markers during infection. The platelet counts did not differ between WT and *Alox12* KO mice throughout infection (*SI Appendix*, Fig. S4*D*). We observed a reduction in the number of activated platelets on the 5th day postinfection in the Alox12 KO group, specifically in male mice (Fig. 4*D*). Additionally, we found a decrease in the production of platelet factor 4 (CXCL4) in the lungs of KO mice on the 3rd day postinfection (*SI Appendix*, Fig. S4*F*), further supporting the reduced platelet activation in these mice. This decline in platelet activation aligns with prior research findings indicating that 12-HETE, the primary metabolite of 12-LOX, serves as a platelet activator (15, 23–25). Additionally, we assessed immune cell counts in whole blood, finding no significant changes among analyzed groups (*SI Appendix*, Fig. S5).

As evidenced in previous studies, SARS-CoV-2 infection in K18-hACE-2 mice is associated with the recruitment of inflammatory cells to the lung tissue, a rise in inflammatory mediators that leads to serious lung damage (29, 53). When assessing the influence of 12-LOX on this pathogenic process, we noted an increased inflammatory score in the lungs of the *Alox12* KO group following infection (Fig. 4*E*). This was characterized by more severe lung injury, significant leukocyte infiltration, thickened alveolar walls, and reduced alveolar spaces on both 3 and 5 d postinfection (Fig. 4*F*). Despite the roles of 12-LOX role in platelet activation, we observed no signs of higher coagulation processes in the pulmonary tissues of KO animals. We also evaluated the plasma D-dimer levels in mice on days 1, 3, and 5 postinfection, as well as in mock groups, and did not observe a significant increase in D-dimer production in any of the tested groups (*SI Appendix*, Fig. S4*E*). Peribranchial and alveolar lung regions were analyzed by immunofluorescnes to detect CD3+, granulocytes (Ly6G+/Ly6C+) and macrophages (F4/80+). As depicted in Fig. 4*G*, there was an increase in lymphocyte counts on days 3 and 5 postinfection in *Alox12* KO-infected mice compared to mock-infected mice. Furthermore, infection led to an increase in CD3+ T cells on day 5 in the *Alox12* KO mice relative to WT mice. Granulocyte counts were also elevated on day 3 in the infected groups, with a higher quantity observed in the *Alox12* KO group on day 5 postinfection. We observed a progressive accumulation of macrophages throughout the infection, but there was no significant difference between the infected groups (Fig. 4*G*).

We next correlated the LMI produced during SARS-CoV-2 infection and the histopathological scores in the lungs. The Spearman correlation analysis revealed a significant positive correlation with the expression of the lipids PGE_2 and TXA_2, assessed by quantitating TXB_2 (Fig. 4*G* and *SI Appendix*, Fig. S6). The increased levels of these lipids in cases of more severe SARS-CoV-2 infections have been previously demonstrated (17–19). Neutrophil 12-LOX-deficient animals also showed an elevation of PGE_2 in the lungs (28). One 12-LOX metabolite, 12-HETrE, was negatively correlated with the inflammatory scores (Fig. 4*H* and *SI Appendix*, Fig. S6). Consistent with these results, more severe inflammatory scores were observed in *Alox12* KO mice that produce little or no 12-HETrE. This comprehensive analysis contributes to our understanding of the intricate interplay between lipid mediators and enzyme regulation during SARS-CoV-2 infection, shedding light on the complex dynamics of the host response.

To determine whether the results obtained were specific to *Alox12* KO mice, we generated two additional mouse lines (K18-ACE2/*Txas1* KO and K18-ACE2/*Tph1* KO) deficient for enzymes associated with platelet biology. Platelets are a major producer of TXA_2 with the thromboxane synthase 1 (TXAS 1) enzyme being essential for TXA_2 production following AA metabolism by COX. Platelets are also an important storage site for serotonin that is released during aggregation and vasoconstriction, where it then acts as an agonist to other platelets (33). Tryptophan hydroxylase 1 (Tph1) oxidizes L-tryptophan to 5-hydroxy-l-tryptophan in the rate-determining step of serotonin biosynthesis. K18-ACE2/*Txas1* KO and K18-ACE2/*Tph1* KO were generated and infected with SARS-CoV-2, with severity of disease assessed. We observed no significant differences in lethality, weight loss, or viral load between KO animals and the control group, arguing specificity for the *Alox12* KO genotype (*SI Appendix*, Fig. S7). It is important to consider that the results observed using the Txas1 KO might be due to a shift in the metabolism of AA toward other prostanoids, such as PGE2, confounding the real effect of TXA2.

Additionally, we tested the infection of the Alox12 KO mice used in this work using a different virus, Influenza virus H1N1 that alike SARS-CoV-2, causes a severe pulmonary infection. Infected mice displayed signs of infection such as weight loss, lung viral loads, and reach of endpoint limits. Both WT and *Alox12* KO mice experienced a similar course of infection with H1N1 with no apparent differences between mouse genotypes. These results suggest that the increased susceptibility of *Alox12* KO mice is specific to SARS-CoV-2. (*SI Appendix*, Fig. S7).

Discussion

In the context of SARS-CoV-2 infection, where exacerbated inflammation is a determining factor of viral pathogenesis, understanding the role of LMI, is essential. Efforts have been made in recent years to document the changes in these mediators during SARS-CoV-2 infection (17, 18, 54). In this study, we illustrate that SARS-CoV-2 disease severity is exacerbated in both $cPLA_2\alpha$ KO-deficient and platelet 12-LOX-deficient mice. Mice deficient for $cPLA_2\alpha$ did not show reduced levels of AA in lung homogenates relative to WT mice suggesting that other enzymes in the lungs are responsible for AA release. In fact, a paper by Nomura et al reported that the source of AA varies depending on the tissue with liver and lungs relying more on mono acyl glycerol (MAG) lipase (and the hydrolysis of 2-arachidonoyl-glycerol) in LPS-treated mice rather than $cPLA_2\alpha$ activity for the generation of AA (55). Mice deficient for $cPLA_2\alpha$ showed signs of increased disease severity characterized by higher lung inflammatory scores and cytokine production. However, the only lipids significantly affected by the KO were the release of EPA and the associated biosynthesis of PGE_3. Interestingly, when we assessed the levels of LMI in the lung of severe COVID-19 patients (17), the only PUFA whose levels were not increased compared to healthy controls was EPA. Assuming that EPA release is also the consequence of $cPLA_2\alpha$ in

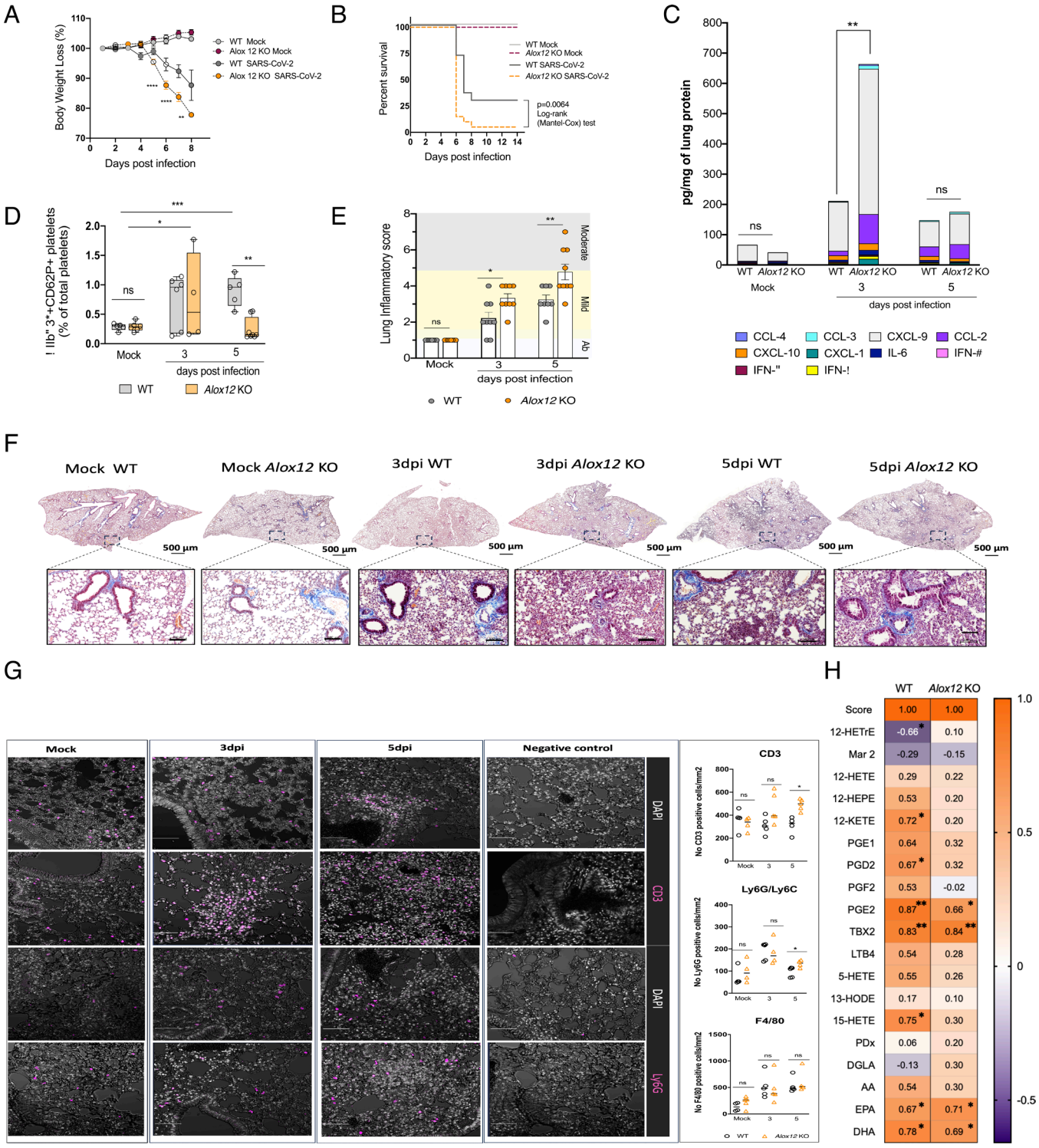

Fig. 4. 12-LOX deficiency increases disease severity and lung inflammation after SARS-CoV-2 infection. Nine-wk-old WT and *Alox12* KO mice were inoculated intranasally with 500 $TCID_{50}$/25 µL. (*A*) Changes in body weight during the infection course. The data are expressed as the mean ± SEM. From days 1 to 8 postinfection, differences were evaluated using a Two-way ANOVA followed by Fisher's LSD test (n = 10 to 20). (*B*) Kaplan–Meier survival curve of WT and *Alox12* KO-infected mice with 500 $TCID_{50}$ of SARS-CoV-2/mouse (n = 10 to 20). Lungs of mock- or SARS-CoV-2-infected mice were collected on days 3 and 5 postinfection. (*C*) The sum of the concentrations of key inflammatory cytokines was determined in lung homogenates through multiplex cytokine quantification (pg/mg of lung protein) in mock, 3, and 5 d postinfection groups (n = 10). (*D*) Whole blood male mice platelets activation determined by flow cytometry in mock, 3 and 5 d postinfection groups (n = 5 to 8). (*E*) Assessment of lung inflammation scores across different groups. (n = 8 to 9). (*F*) Mouse lung sections stained by Carstairs staining highlighting the general histological changes across the experimental groups. (*G*) Leukocytes density per lung area (mm^2) among groups. Leukocytes were stained for CD3, Ly6G/Ly6C, and F4/80 markers and analyzed by confocal microscopy (n = 4 to 5). (*H*) Correlation heatmap displaying Spearman correlation coefficients between histopathological inflammatory scores and LMI dose (pmol/mg of lung protein). The color legend on the left side of the map illustrates Spearman correlation coefficients, while asterisks denote calculated *P* values. A *P* value < 0.05 was accepted as significant. Statistical differences were analyzed by ordinary one-way ANOVA plus Fisher's LSD test. Nonparametric comparisons were conducted using the Kruskal–Wallis test with Dunn's posttest. ns: nonstatistically significant. *$P < 0.05$; **$P < 0.005$; ****$P < 0.0001$.

humans, we speculate that in both species the role of $cPLA_2\alpha$ is limited during the inflammatory phase of COVID-19. This agrees with a recent study from COVID-19 patients highlighting that the increases in PGD_2, PGI_2, and 12-HETE correlated with $sPLA_2$ enzymes, supporting a lack of critical involvement of $cPLA_2\alpha$ during COVID-19 (56).

The 12-LOX platelet enzyme is responsible for the production of biolipids that can play a regulatory role both within the platelet itself as well as at distal tissues and organ systems (15, 57). The main metabolite produced by 12-LOX is 12(S)-HETE that mediates various functions including the activation of platelet functions (23), and the regulation of proinflammatory mediators' production mediated by a signaling axis involving the receptor GPR31 (58). Using *Alox15* KO mice that are deficient for 12(S)-HETE production by neutrophils, Pernet et al demonstrated greater inflammatory responses and susceptibility to influenza and SARS-CoV-2 infections. Administration of 12(S)-HETE or 15-HETE had no impact on disease outcome arguing that other LMI derived from 12/15-LOX pathway might provide protection (28). Our results show that deficiency in the antiplatelet 12-HETrE exhibits a strong negative and significant correlation with the mouse inflammatory scores and would argue for a role of 12-HETrE in regulating the inflammation induced by SARS-CoV-2 infection. Despite being recognized for its anticoagulant activity, 12-HETrE potential anti-inflammatory modulatory effects require further investigation (27). Ikei et al. (2014) demonstrated in vitro that the presence of 12-HETrE can inhibit the small GTPase Rap1 activity. Platelet activation and regulation of endothelial barrier function are controlled by Rap1 (23, 59). As this protein regulates others in the Rho signaling pathway, it is possible that the products of 12-LOX are associated with the differential expression of Rho genes observed in platelet RNAseq data (Fig. 3*G*). Despite this evidence, the intricate interrelation among LMI makes it challenging to determine whether any single one is more relevant to the observed phenotype or whether their synergistic action is necessary.

Additionally, Mar2 and PDx, specialized proresolving mediators synthesized from DHA (60, 61) also exhibited reduced levels in the KO groups after infection. This suggests that Mar2 and PDx, when present at sufficient levels, might be beneficial in diminishing the severity of the inflammatory response triggered by SARS-CoV-2 although the levels that we quantitated might not be sufficient for promoting such an effect. Other 12-LOX-derived oxylipins, notably 12-KETE, whose functions remain undefined (62), were also less produced in the *Alox12* KO groups.

A study published in 2023 analyzing lipids in human plasma and urine samples from COVID-19 patients showed that the elevation in PGD2, PGI2, and 12-HETE correlated with sPLA2 and disease severity (56). In our study, we also observed that AA metabolites produced via COX1 were elevated in mice with greater lung inflammation. However, such correlation was not observed for 12-HETE in our study. The KO of 12-LOX in platelets altered the levels of various bioactive lipids in the lungs of the animals, and the overall effect of these changes was an increase in inflammation. However, we cannot attribute this phenotype to the increase of one or two lipids in isolation without considering the overall context of lipid modification.

Lung RNAseq analyses showed changes in genes associated with the inflammasome complex, particularly the NLRP1 inflammasome (Fig. 3 *B*–*D*). Notably, we observed a downregulation of the nrlp1a gene and upregulation of *Nrlp1b* within the NLRP1 complex, in *Alox12* KO mice (Fig. 3*F*). NLRP1 acts as a highly expressed and functional direct sensor for RNA virus infection in epithelial tissues. Upon activation, it forms the inflammasome, a multiprotein immune effector complex. Inflammasome assembly activates caspase-1, resulting in the secretion of proinflammatory cytokines such as IL-1β and IL-18. Additionally, it activates the pore-forming protein Gasdermin-D, inducing pyroptotic cell death. Proper regulation of these signaling activation processes is crucial for their beneficial effects against infection (51).

Studies have linked the inflammatory response from NLRP3 inflammasome activation to the severity of SARS-CoV-2 infection (63, 64). The relationship with the NLRP1 inflammasome complex remains unclear. Recently, one study demonstrated that SARS-CoV-2 infection activates human NLRP1 inflammasome in epithelial cells which triggers inflammasome assembly and cell death and limits the production of infectious viral particles, potentially providing benefits during infection (65). Of potential interest, specialized proresolving mediators such as Resolvins D2 (a product derived from DHA) were shown to inhibit Nlrp3 (66). Work is currently underway to understand how 12-LOX deficiency might lead to *Nlrp1b* gene activation.

We observed that the absence of platelet 12-LOX leads to alterations in the pulmonary inflammatory profile, ultimately resulting in the early demise of mice following SARS-CoV-2 infection. The intensification of lung inflammation is characterized by increased production of proinflammatory cytokines and chemokines, mainly from day 3 after infection. This is accompanied by an early peak in pulmonary inflammatory scores, along with an increase in infiltration of cells positive for CD3 and Ly6G/Ly6C in the lungs.

Prostaglandins play a critical role in inflammatory settings and have been explored in the pathogenesis of coronaviruses. PGE_2 regulates stress responses, immunity, and inflammatory pathways but has been described as contributing to an impaired immune response to COVID-19 infection (2). $PGF_{2\alpha}$ and PGD_2 subclasses are associated with proinflammatory responses, with the action of PGD_2 contributing to the increased severity of SARS-CoV-2 infection in middle-aged mice (54). Our study revealed an increase in prostaglandin production throughout the infection, with PGE_2 and TXA_2 (assessed by quantitating TXB_2) showing a positive correlation with lung inflammation, as demonstrated in other studies (17, 18, 54). However, the *Alox12* KO generated modest modulations of the tested prostaglandins and TXB_2 that are not sufficient to explain the worse outcome observed. Furthermore, disease severity in *Txas1* KO mice was similar to that of WT mice arguing against TXA2 playing major contributions to disease in our system. The lipid profile indicates that the pathways of 12-LOX, 5-LOX, and 15-LOX, which are regulated by 12-LOX products, also contribute to the distinctive lipid signature observed. The decrease in antiplatelet or anti-inflammatory lipids (12-HEPE, 12-HETrE, 15(S)-HETE, 13-HODE, 12-HETE, and PDx) may synergistically contribute to the *Alox12* KO phenotype. Despite observing greater tissue inflammation in the lungs of KO mice, a lower production of LTB_4, a potent LMI promoting the migration of myeloid leukocytes into tissues, was noted. This is somewhat counterintuitive given that we observed an increased number of neutrophils in *Alox12*-deficient mice and that 5-LOX and not 12-LOX is chiefly mediating LTB_4 biosynthesis. This suggests that 1) during SARS-CoV-2 infection, LTB_4 does not actively participate to neutrophil recruitment; 2) the decreased LTB_4 levels in *Alox12*-deficient mice might be the consequence of a dramatic decrease in 12-HpETE levels, the latter stimulating LTB_4 biosynthesis through transcellular processes (67); and that 3) innate immune cells might be less capable, despite their increased number, of clearing viruses/debris, given the strong involvement of LTB_4 at stimulating host defense-related functions.

In summary, our findings underscore the intricate interplay between platelet-type 12-LOX-related lipid metabolism and inflammatory responses during SARS-CoV-2 infection, providing valuable insights into potential therapeutic targets for mitigating severe outcomes. Our results would suggest that administration of 12-HETrE or analogs thereof, such as CS585, might prove beneficial for the treatment of infections associated with hyperinflammation (68).

Limitations of the Study

Our study aimed to comprehend the contribution of 12-LOX to the SARS-CoV-2 pathogenesis in mice. The extrapolation of our findings to the physiology of 12-LOX in humans must consider species-specific variations in the products formed by 12-LOX and 15-LOX. Furthermore, the *Alox12* gene also encodes the production of 12-LOX in the skin of humans and mice, and the relevance of this aspect was not investigated in our study. 12-HETE and 15(S)-HETE can be esterified in membrane phospholipids, which may limit the use of their free levels as a reliable index of their generation. This potential esterification should be considered when interpreting the data on their free concentrations. Another limitation of our study lies in the animal model and viral strain used. The K18-ACE2 mice have an ACE2 receptor distribution that is much wider than what is observed in humans expanding the natural tropism of the virus. Finally, the SARS-CoV-2 Delta variant used in this study is more virulent than many other SARS-CoV-2 strains, including the more prevalent Omicron-derived viruses. The contributions of 12-LOX metabolites in milder SARS CoV-2 infections remain to be determined.

Data, Materials, and Software Availability. All data have been deposited in Figshare (https://figshare.com/articles/dataset/Deficiency_in_Platelet_12-Lipoxygenase_Exacerbates_Inflammation_and_Disease_Severity_During_SARS-CoV-2_Infection_data_xlsx/28439642?file=52453313) (69).

ACKNOWLEDGMENTS. This study was supported by a CIHR grant (#172632) awarded to N.F., E.B., and LF and by the Coronavirus Variants Rapid Response Network grant (#GA1-117694) awarded to L.F. We thank the next-generation sequencing core facility of the CHU de Quebec Research for their excellent service and expertise.

Author affiliations: [a]Division of Infectious and Immune Diseases, Centre de Recherche du Centre Hospitalier Universitaire de Québec-Université Laval, Québec City, QC G1V 4G2, Canada; [b]Division of Reproduction, mother and youth health, Centre de Recherche du Centre Hospitalier Universitaire de Québec-Université Laval, Québec City, QC G1V 4G2, Canada; [c]Morphology Department, Universidade Federal de Minas Gerais, Belo Horizonte 31270-901, Brazil; [d]Division of Endocrinology and Nephrology, Centre de Recherche du Centre Hospitalier Universitaire de Québec-Université Laval, Québec City, QC G1V 4G2, Canada; [e]Centre de recherche de l'Institut Universitaire de cardiologie et pneumologie de Québec, Division of pneumology, Faculty of medicine, Université Laval, Québec City, QC G1V 4G5, Canada; [f]Canada Excellence Research Chair on the Microbiome-Endocannabinoidome Axis in Metabolic Health, Université Laval, Québec City, QC G1V 4G5, Canada; [g]Centre de Recherche ARThrite–Arthrite, Recherche, Traitements, Université Laval, Québec, QC G1V 4G2, Canada; and [h]Department of microbiology, infectious disease and immunology, Faculty of Medicine, Université Laval, Québec City, QC G1V 0A6, Canada

1. N. Zhu *et al.*, A novel coronavirus from patients with pneumonia in China, 2019. *N. Engl. J. Med.* **382**, 727–733 (2020).
2. P. K. Bhatraju *et al.*, Covid-19 in critically ill patients in the Seattle region–Case series. *N. Engl. J. Med.* **382**, 2012–2022 (2020).
3. N. Tang, D. Li, X. Wang, Z. Sun, Abnormal coagulation parameters are associated with poor prognosis in patients with novel coronavirus pneumonia. *J. Thromb. Haemost.* **18**, 844–847 (2020).
4. M. Levi, J. Thachil, T. Iba, J. H. Levy, Coagulation abnormalities and thrombosis in patients with COVID-19. *Lancet Haematol.* **7**, e438–e440 (2020).
5. K. B. Manne, Platelet gene expression and function in patients with COVID-19. *Ann. Oncol.* **7**, 19–21 (2020).
6. Y. Zaid *et al.*, Platelets can associate with SARS-CoV-2 RNA and are hyperactivated in COVID-19. *Circ. Res.* **127**, 1404–1418 (2020).
7. F. Puhm *et al.*, Platelet activation by SARS-CoV-2 implicates the release of active tissue factor by infected cells. *Blood Adv.* **6**, 3593–3605 (2022).
8. J. P. Bernardes *et al.*, Longitudinal multi-omics analyses identify responses of megakaryocytes, erythroid cells, and plasmablasts as hallmarks of severe COVID-19. *Immunity* **53**, 1296–1314.e9 (2020).
9. H. N. Hotz, Christa L. Walker, Igor Rudan, L. Liu, Platelet activation and platelet-monocyte aggregate formation trigger tissue factor expression in patients with severe COVID-19. *Ann. Oncol.* **7**, 19–21 (2020).
10. M. Koupenova, L. Clancy, H. A. Corkrey, J. E. Freedman, Circulating platelets as mediators of immunity, inflammation, and thrombosis. *Circ. Res.* **122**, 337–351 (2018).
11. L. Guo, M. T. Rondina, The era of thromboinflammation: Platelets are dynamic sensors and effector cells during infectious diseases. *Front. Immunol.* **10**, 2204 (2019).
12. L. S. Portier Sfeir, Agnel and Symington, Role of platelets in detection and regulation of infection. *Physiol. Behav.* **176**, 139–148 (2021).
13. F. Cognasse *et al.*, Evidence of Toll-like receptor molecules on human platelets. *Immunol. Cell Biol.* **83**, 196–198 (2005).
14. I. Gautam *et al.*, From classical to unconventional: The immune receptors facilitating platelet responses to infection and inflammation. *Biology (Basel)* **9**, 343 (2020).
15. J. Yeung *et al.*, Platelet 12-LOX is essential for FcγRIIa-mediated platelet activation. *Blood* **124**, 2271–2279 (2014).
16. V. B. O'Donnell, R. C. Murphy, S. P. Watson, Platelet lipidomics: Modern day perspective on lipid discovery and characterization in platelets. *Circ. Res.* **114**, 1185–1203 (2014).
17. A. Archambault *et al.*, High levels of eicosanoids and docosanoids in the lungs of intubated COVID-19 patients. *FASEB J.* **35**, e21666 (2021).
18. I. Dubuc *et al.*, Cytokines and lipid mediators of inflammation in lungs of SARS-CoV-2 infected mice. *Front. Immunol.* **13**, 893792 (2022).
19. R. Ravindran *et al.*, Lipid mediators and cytokines/chemokines display differential profiles in severe versus mild/moderate COVID-19 patients. *Int. J. Mol. Sci.* **24**, 13054 (2023).
20. E. Lefrançais *et al.*, The lung is a site of platelet biogenesis and a reservoir for haematopoietic progenitors. *Nature* **544**, 105–109 (2017).
21. Z. Ma, J. Turk, The molecular biology of the group VIA Ca2+-independent phospholipase A2. *Prog. Nucleic Acid Res. Mol. Biol.* **67**, 1–33 (2001).
22. B. E. Tourdot, M. Holinstat, Targeting 12-lipoxygenase as a potential novel antiplatelet therapy. *Trends Pharmacol. Sci.* **38**, 1006–1015 (2017).
23. K. N. Ikei *et al.*, Investigations of human platelet-type 12-lipoxygenase: Role of lipoxygenase products in platelet activation. *J. Lipid Res.* **53**, 2546–2559 (2012).
24. J. Yeung *et al.*, 12-lipoxygenase activity plays an important role in PAR4 and GPVI-mediated platelet reactivity. *Thromb. Haemost.* **110**, 569–581 (2013).
25. R. Adili *et al.*, First selective 12-LOX inhibitor, ML355, impairs thrombus formation and vessel occlusion in vivo with minimal effects on hemostasis. *Arterioscler. Thromb. Vasc. Biol.* **37**, 1828–1839 (2017).
26. A. Schafer, Deficiency of platelet lipoxygenase activity in myeloproliferative disorders. *Med. Sci. Sports Exerc.* **314**, 605–613 (1994).
27. J. Yeung *et al.*, 12-HETrE, a 12-LOX oxylipin of DGLA, inhibits thrombosis via Gαs signaling in platelets. *Arterioscler. Thromb. Vasc. Biol.* **36**, 2068–2077 (2016).
28. E. Pernet *et al.*, Neonatal imprinting of alveolar macrophages via neutrophil-derived 12-HETE. *Nature* **614**, 530–538 (2023).
29. E. S. Winkler *et al.*, SARS-CoV-2 infection of human ACE2-transgenic mice causes severe lung inflammation and impaired function. *Nat. Immunol.* **21**, 1327–1335 (2020).
30. É. Lacasse *et al.*, SARS-CoV-2 Nsp2 contributes to inflammation by activating NF-κB. *Viruses* **15**, 334 (2023).
31. E. Boilard *et al.*, Influenza virus H1N1 activates platelets through FcRIIA signaling and thrombin generation. *Blood* **123**, 2854–2863 (2014).
32. H. Uozumi *et al.*, Role of cytosolic phospholipase A2 in allergic response and parturition. *Nature* **390**, 618–622 (1997).
33. F. Côté *et al.*, Disruption of the nonneuronal tph1 gene demonstrates the importance of peripheral serotonin in cardiac function. *Proc. Natl. Acad. Sci. U. S. A.* **100**, 13525–13530 (2003).
34. G. Campolina-Silva *et al.*, Dietary vitamin D mitigates coronavirus-induced lung inflammation and damage in mice. *Viruses* **15**, 2434 (2023).
35. G. Kärber, Beitrag zur kollektiven Behandlung pharmakologischer Reihenversuche. *Archiv. f. Experiment. Pathol. u. Pharmakol.* **162**, 480–483 (1931).
36. C. Carstairs, The identification of platelets and platelet antigens in histological sections. *J. Pathol. Bacteriol.* **90**, 225–231 (1965).
37. J. C. Horvat *et al.*, Neonatal chlamydial infection induces mixed T-cell responses that drive allergic airway disease. *Am. J. Respir. Crit. Care Med.* **176**, 556–564 (2007).
38. N. L. Bray, H. Pimentel, P. Melsted, L. Pachter, Near-optimal probabilistic RNA-seq quantification. *Nat. Biotechnol.* **34**, 525–527 (2016).
39. M. I. Love, W. Huber, S. Anders, Moderated estimation of fold change and dispersion for RNA-seq data with DESeq2. *Genome Biol.* **15**, 1–21 (2014).
40. Z. Gu, R. Eils, M. Schlesner, Complex heatmaps reveal patterns and correlations in multidimensional genomic data. *Bioinformatics* **32**, 2847–2849 (2016).
41. A. Archambault *et al.*, Biosynthesis of the novel endogenous 15-lipoxygenase Metabolites N-13-Hydroxy-octodecadienoyl-ethanolamine and 13-hydroxy-octodecadienoyl-glycerol by human neutrophils and eosinophils. *Cells* **10**, 2322 (2021).
42. J. Xia, I. V. Sinelnikov, B. Han, D. S. Wishart, MetaboAnalyst 3.0-making metabolomics more meaningful. *Nucleic Acids Res.* **43**, W251–W257 (2015).
43. J. Xia, N. Psychogios, N. Young, D. S. Wishart, MetaboAnalyst: A web server for metabolomic data analysis and interpretation. *Nucleic Acids Res.* **37**, 652–660 (2009).
44. M. Z. Tay, C. M. Poh, L. Rénia, P. A. MacAry, L. F. P. Ng, The trinity of COVID-19: Immunity, inflammation and intervention. *Nat. Rev. Immunol.* **20**, 363–374 (2020).
45. L. Yang *et al.*, COVID-19: Immunopathogenesis and immunotherapeutics. *Signal Transduct. Target Ther.* **5**, 128 (2020).
46. A. C. Duchez *et al.*, Platelet microparticles are internalized in neutrophils via the concerted activity of 12-lipoxygenase and secreted phospholipase A2-IIA. *Proc. Natl. Acad. Sci. U.S.A.* **112**, E3564–E3573 (2015).
47. A. Kulkarni, J. L. Nadler, R. G. Mirmira, I. Casimiro, Regulation of tissue inflammation by 12-lipoxygenases. *Biomolecules* **11**, 717 (2021).

48. Y. B. Jarrar *et al.*, Identification of cytochrome P450s involved in the metabolism of arachidonic acid in human platelets. *Prostaglandins Leukot. Essent. Fatty Acids* **89**, 227–234 (2013).
49. W. S. Powell, J. Rokach, Biosynthesis, biological effects, and receptors of hydroxyeicosatetraenoic acids (HETEs) and oxoeicosatetraenoic acids (oxo-ETEs) derived from arachidonic acid. *Biochim. Biophys. Acta Mol. Cell Biol. Lipids* **1851**, 340–355 (2015).
50. V. B. O'Donnell *et al.*, Failure to apply standard limit-of-detection or limit-of-quantitation criteria to specialized pro-resolving mediator analysis incorrectly characterizes their presence in biological samples. *Nat. Commun.* **14**, 10–14 (2023).
51. P. S. Mitchell, A. Sandstrom, R. E. Vance, The NLRP1 inflammasome: New mechanistic insights and unresolved mysteries. *Curr. Opin. Immunol.* **60**, 37–45 (2019).
52. E. Kerkelä *et al.*, Exploring transcriptomic landscapes in red blood cells, in their extracellular vesicles and on a single-cell level. *Int. J. Mol. Sci.* **23**, 12897 (2022).
53. K. S. Lee *et al.*, SARS-CoV-2 Delta variant induces enhanced pathology and inflammatory responses in K18-hACE2 mice. *PLoS One* **17**, e0273430 (2022).
54. L. Y. R. Wong *et al.*, Eicosanoid signalling blockade protects middle-aged mice from severe COVID-19. *Nature* **605**, 146–151 (2022).
55. D. K. Nomura *et al.*, Endocannabinoid hydrolysis generates brain prostaglandins that promote neuroinflammation. *Science* **334**, 809–813 (2012).
56. H. Meng *et al.*, Deep phenotyping of the lipidomic response in COVID-19 and non-COVID-19 sepsis. *Clin. Transl. Med.* **13**, e1440 (2023).
57. M. Chatterjee, Platelet lipidome: Dismantling the "Trojan horse" in the bloodstream. *J. Thromb. Haemost.* **18**, 543–557 (2020).
58. X. J. Zhang *et al.*, An ALOX12-12-HETE-GPR31 signaling axis is a key mediator of hepatic ischemia-reperfusion injury. *Nat. Med.* **24**, 73–83 (2018).
59. W. J. Pannekoek, A. Post, J. L. Bos, Rap1 signaling in endothelial barrier control. *Cell Adh. Migr.* **8**, 100–107 (2014).
60. T. V. Hansen, A. Vik, C. N. Serhan, The protectin family of specialized pro-resolving mediators: Potent immunoresolvents enabling innovative approaches to target obesity and diabetes. *Front. Pharmacol.* **9**, 1582 (2019).
61. B. Deng *et al.*, Maresin biosynthesis and identification of maresin 2, a new anti-inflammatory and pro-resolving mediator from human macrophages. *PLoS One* **9**, e102362 (2014).
62. L. Stanger, M. Holinstat, Bioactive lipid regulation of platelet function, hemostasis, and thrombosis. *Pharmacol. Ther.* **246**, 108420 (2023).
63. N. Zhao, B. Di, L. li Xu, The NLRP3 inflammasome and COVID-19: Activation, pathogenesis and therapeutic strategies. *Cytokine Growth Factor Rev.* **61**, 2–15 (2021).
64. P. Pan *et al.*, SARS-CoV-2 N protein promotes NLRP3 inflammasome activation to induce hyperinflammation. *Nat. Commun.* **12**, 4664 (2021).
65. R. Planès *et al.*, Human NLRP1 is a sensor of pathogenic coronavirus 3CL proteases in lung epithelial cells. *Mol. Cell* **82**, 2385–2400.e9 (2022).
66. A. Lopategi *et al.*, Frontline science: Specialized proresolving lipid mediators inhibit the priming and activation of the macrophage NLRP3 inflammasome. *J. Leukoc. Biol.* **105**, 25–36 (2019).
67. J. Maclouf, B. Fruteau De Laclos, P. Borgeat, Stimulation of leukotriene biosynthesis in human blood leukocytes by platelet-derived 12-hydroperoxy-icosatetraenoic acid. *Proc. Natl. Acad. Sci. U.S.A.* **79**, 6042–6046 (1982).
68. L. Stanger *et al.*, The oxylipin analog CS585 prevents platelet activation and thrombosis through activation of the prostacyclin receptor. *Blood* **142**, 1556–1569 (2023).
69. A. C. d. S. P. Andrade *et al.*, Date from "Deficiency in platelet 12-lipoxygenase exacerbates inflammation and disease severity during SARS-CoV-2 infection." Figshare. https://figshare.com/articles/dataset/Deficiency_in_Platelet_12-Lipoxygenase_Exacerbates_Inflammation_and_Disease_Severity_During_SARS-CoV-2_Infection_data_xlsx/28439642?file=52453313. Deposited 18 February 2025.